Applied Catalysis B: Environmental 320 (2023) 121954

Contents lists available at ScienceDirect

Applied Catalysis B: Environmental

journal homepage: www.elsevier.com/locate/apcatb

Enhanced support effects in single-atom copper-incorporated carbon nitride for photocatalytic suzuki cross-coupling reactions

Chenhui Han [a,b], Ruijuan Qi [c], Ruolun Sun [b], Kaicai Fan [d], Bernt Johannessen [e], Dong-Chen Qi [b], Shaowen Cao [f,*], Jingsan Xu [b,*]

[a] School of Chemistry and Chemical Engineering, Inner Mongolia University, Hohhot, Inner Mongolia 010021, PR China
[b] School of Chemistry and Physics, Science and Engineering Faculty, Queensland University of Technology, Brisbane, QLD 4000, Australia
[c] Key Laboratory of Polar Materials and Devices, Ministry of Education, Department of Electronics, East China Normal University, Dongchuan Road 500, Shanghai 200241, PR China
[d] Centre for Catalysis and Clean Energy, School of Environment and Science, Griffith University, Queensland 4222, Australia
[e] Australian Synchrotron, Australia's Nuclear Science and Technology Organisation, Victoria 3168, Australia
[f] State Key Laboratory of Advanced Technology for Materials Synthesis and Processing, Wuhan University of Technology, 122 Luoshi Road, Wuhan 430070, PR China

ARTICLE INFO

Keywords:
Single-atom copper
Carbon nitride
Support effect
Photocatalysis
Suzuki cross-coupling

ABSTRACT

Conditioning the nature of metal active sites for better performance by well designing and constructing the support material is always appealing in heterogeneous catalysis. Herein, Cu species was introduced into the bulk phase of carbon nitride to strengthen the interlayer connection and optimize the electronic structure. The resulting material (CN-Cu) demonstrated an enhanced support effect for Pd catalyzed Suzuki cross-coupling reactions under light illumination. Detailed characterizations showed that Cu species were atomically incorporated in intra/interlayer of CN framework through coordinating with pyridinic nitrogen, leading to improved light absorption and more efficient charge carrier transfer. More importantly, the electronic effect of CN-Cu to the surface Pd was enhanced by the electron drift from Cu to N, thereby rendered an electron-rich Pd surface. Such Pd surfaces allowed faster electron injection from Pd(0) to the LUMO of aryl halides and therefore accelerate the rate-determining step of the coupling reaction.

1. Introduction

In heterogeneous catalysis, the catalyst supports often play a critical role in determining the efficiency of metal active centres through the so-called support effects which are always appealing and attractive in catalysis studies. Since the metal species are normally anchored by the structural surface defects of support via complex interactions, supports can be regarded as a macromolecular ligand for metal reactive centres [1–5]. In this scenario, the property of supports not only determines the dispersion dimensions (i.e. nanoparticles, clusters, or single metal atoms) of metal species through geometric effects and confinement effects; more importantly, it significantly affects the electronic states of reactive sites by contributing or withdrawing electrons through electronic effects, by which the affinity between metal active centres and reaction substrates or intermediates could be altered, therefore changing the catalytic performance [2,3,5–8]. In this context, one can condition the nature of active sites and improve their performances in catalysis by well designing and constructing the support material.

Polymeric carbon nitride (CN) as a two-dimensional organic semiconductor has been widely used as support material in catalysis [9–19]. Customizing CN structure to adapt various catalytic metal species is another promising way of realizing better performance that differs from directly optimizing catalytic active sites. Benefiting from the abundant coordination sites on framework, CN is capable of immobilizing various single atom metals in inter/intralayers, depending on the synthesis approaches [13,20–22]. There have been multiple case studies investigated the performance of single-atom metal anchored at CN surface for catalysis, whereas the role played by the metal species in bulk phase is rarely reported, although they have been found effective in constructing interlayer electronic channels and changing the electronic structure of CN material, and therefore may potentially affect the surface active sites through support effects [23–31]. Fu et al. and Peng et al. reported single-atom-Cu doped CN material for different reactions. However, the role of bulk phase Cu is elusive because the surface Cu was served as the

* Corresponding authors
E-mail addresses: swcao@whut.edu.cn (S. Cao), Jingsan.xu@qut.edu.au (J. Xu).

https://doi.org/10.1016/j.apcatb.2022.121954
Received 11 July 2022; Received in revised form 21 August 2022; Accepted 4 September 2022
Available online 12 September 2022

catalytic sites in their reactions [22,32].

Herein, to investigate the support effect of CN material with decorated single atomic sites, we developed an easy, liquid-phase preorganization approach for the synthesis of single-atom-Cu-incorporated CN (CN-Cu) and studied its contribution as a support in organic transformations. We selected Pd catalyzed Suzuki cross-coupling as a case study considering the inactivity of the resulted CN-Cu to the reaction and the possibility of intermediate quantification, which allowed us to analyze the support effect from a mechanism point of view.

2. Experimental section

2.1. Sample preparation

2.1.1. Synthesis of CN

polymeric carbon nitride (CN) was synthesized using melamine as the precursor. Typically, 10 g of melamine was placed in a crucible and annealed at 550 °C for 4 h at a heating rate of 2.3 °C/min in nitrogen atmosphere. After cooling down the yellow CN powder was collected.

2.1.2. Synthesis of Cu-incorporated CN (CN-xCu)

Taking CN-2Cu as an example, 2 g of melamine and 151 mg of copper nitrate trihydrate were dissolved in 5 mL methanol and the mixture was shaken for 24 h. After removing the solvent in vacuum, green powder was collected as the precursor. Then the precursor was annealed at 550 °C for 4 h at a heating rate of 2.3 °C/min in nitrogen atmosphere to obtain the CN-2Cu.

2.1.3. Synthesis of Pd/CN and Pd/CN-xCu catalysts

Pd nanoparticles were deposited on CN or CN-xCu via a thermal reduction method in ethanol. Typically, in a round-bottom flask, 200 mg of CN or CN-xCu was pre-dispersed in 100 mL of ethanol by sonicating for 3 h; then desired amount of K_2PdCl_6 solution (0.01 M) was added and stirred for 30 min. Afterwards, 10 mL of water was added, and the mixture was refluxed at 90 °C for 1 h. After cooling down, the sediment was collected, washed twice with ethanol, dried at 60 °C in a vacuum oven and used as catalysts.

2.2. Catalytic activity testing

All the catalytic activity testing were performed in a multichannel photochemical reaction system with controllable light intensity and temperature (PCX-50B Discover, PerfectLight). Typically, 10 mg catalysts, 0.1 mmol 4-iodotoluene, 0.12 mmol phenylboronic acid, 0.3 mmol K_3PO_4, 2 mL solvent (EtOH/H_2O 2:1) were mixed in a 15 mL quartz reactor. The reactor was then sealed, purged with high purity nitrogen, irradiated under light with different wavelength or intensity in the photocatalytic reaction system. The reaction temperature was controlled at 25 °C by colling water. After reaction, the mixture was filtered to remove solid catalysts and then analysed by gas chromatograph equipped with a FID detector.

2.3. The calculation of apparent quantum efficiencies (AQE)

The AQE was calculated according to the following equation,

$$\boldsymbol{AQE} = \frac{n \times V \times (cp,L - cp,D)}{mol\ of\ incident\ photons} \times \mathbf{100}\%,$$

where, n= 1 for this coupling reaction according to the previous report;[33] V is the volume of the reaction system (2 mL); $c_{p,L}$ and $c_{p,D}$ are the product concentration (mol/mL) after light and dark reactions, respectively. The intensity of the incident light was fixed at 15 mW/cm^2; the reaction temperature for both dark and light reactions was controlled at 25 °C by a water-cooling system. The effective area of the quartz window for light transmission is 1.33 cm^2.

3. Results and discussion

3.1. Synthesis of the catalyst supports: single-atom-Cu-incorporated carbon nitride

Fig. 1a illustrates the synthesis of CN-Cu. Briefly, $Cu(NO_3)_2$ was dissolved in methanol as the Cu source, followed by adding melamine under mechanical stirring for preorganization. The colour of the mixture turned from light blue to dark green with stirring, signalling the formation of the Cu-melamine complex precursor. The morphology of the resulted precursor is dependent on the copper source amount: nanofibers were initially formed at low Cu ratios (1 and 2 wt%) and then gradually transformed into a mixture of nanofibers and nanosheets with the increase of Cu content (Fig. 1b-f). The morphology evolvement is supposed to be induced by the newly formed Cu-N coordination bonds, as melamine is prone to coordinate with metal ions such as Ag^+, Cu^{2+} via the pyridinic N atoms forming fibre-like complexes in the form of [M-metal-M], as illustrated in Fig. S1. X-ray powder diffraction pattern (XRD) of the preorganized precursors (Fig. 1g) with different Cu content showed nearly the same diffraction peak position but significantly declined intensity, demonstrating that the precursor did not form a long-range ordered structure, the majority of melamine still existing in the crystal form but with degraded crystallinity. This result is reasonable because melamine was far excessive, with a mole ratio of melamine and $Cu(NO_3)_2$ between 5 and 50. The obtained green powder precursor was then calcinated in argon atmosphere to produce the final product.

The resulted CN-xCu (x = 1, 2, 5, 10, denoting the Cu mass percentage in precursor) samples maintained a typical graphitic carbon nitride framework as reflected by the Fourier-transform infrared spectroscopy (FTIR) measurement (Fig. 2a). The peak at 1627 cm^{-1} can be ascribed to the stretching vibration of C-N groups, and the peaks at 1539, 1399, 1311 and 1223 cm^{-1} derive from the aromatic C-N stretching vibration. The peak at 807 cm^{-1} corresponds to the breathing mode of triazine units [34,35]. The samples showed two-dimensional sheet morphology under high-resolution transmission electron microscopy (HRTEM, Fig. 2b-d), similar to those widely reported graphitic carbon nitride material [14,36]. The nanosheets became curly with the increase of Cu content in samples and there was no Cu nanoparticle observed in all samples. The mass ratios of Cu in the resulted samples were calculated to be 1.47, 2.32, 8.02, and 12.82 wt% for CN-1Cu, CN-2Cu, CN-5Cu, and CN-10Cu, respectively, according to the thermogravimetric analysis (TGA) results (Fig. S2). In all samples, the Cu mass ratios are higher than that in the precursor because of the mass loss (e.g. the loss of -NH_2) of melamine during thermal condensation.

High-angle annular dark-field scanning transmission electron microscopy (HAADF-STEM) gave further information on the structure and composition of these nanosheets (Fig. 3a). Cu species manifested as atomically dispersed bright spots were clearly revealed in the nanosheets, with homogeneous and dense distribution (see the mapping results in Fig. S3). No nanoparticles were found even in high Cu-containing samples (CN-5Cu, Fig. S4), suggesting that the majority of Cu species exist in interlayer and are immobilized by the CN framework. Such a morphology is in sharp contrast to that of the CN supported single-atom metal catalysts, where metal species anchor at surfaces and the metal loading should be very low (normally < 1 wt%) to avoid the formation of nanoparticles [13,17,37]. Besides, the existence of Cu atoms in the interlayer can also be reflected by the XRD patterns of samples. As shown in Fig. 3b, with the increase of Cu contents, the characteristic peak at 27.4° corresponding to the (002) plane of carbon nitride material shifted slightly toward low degrees and weakened, suggesting an expansion of interlayer distance of CN due to the incorporation of Cu atoms.

3.2. Chemical state and local environment of Cu species in the support

To identify the chemical state of Cu species in the samples, we

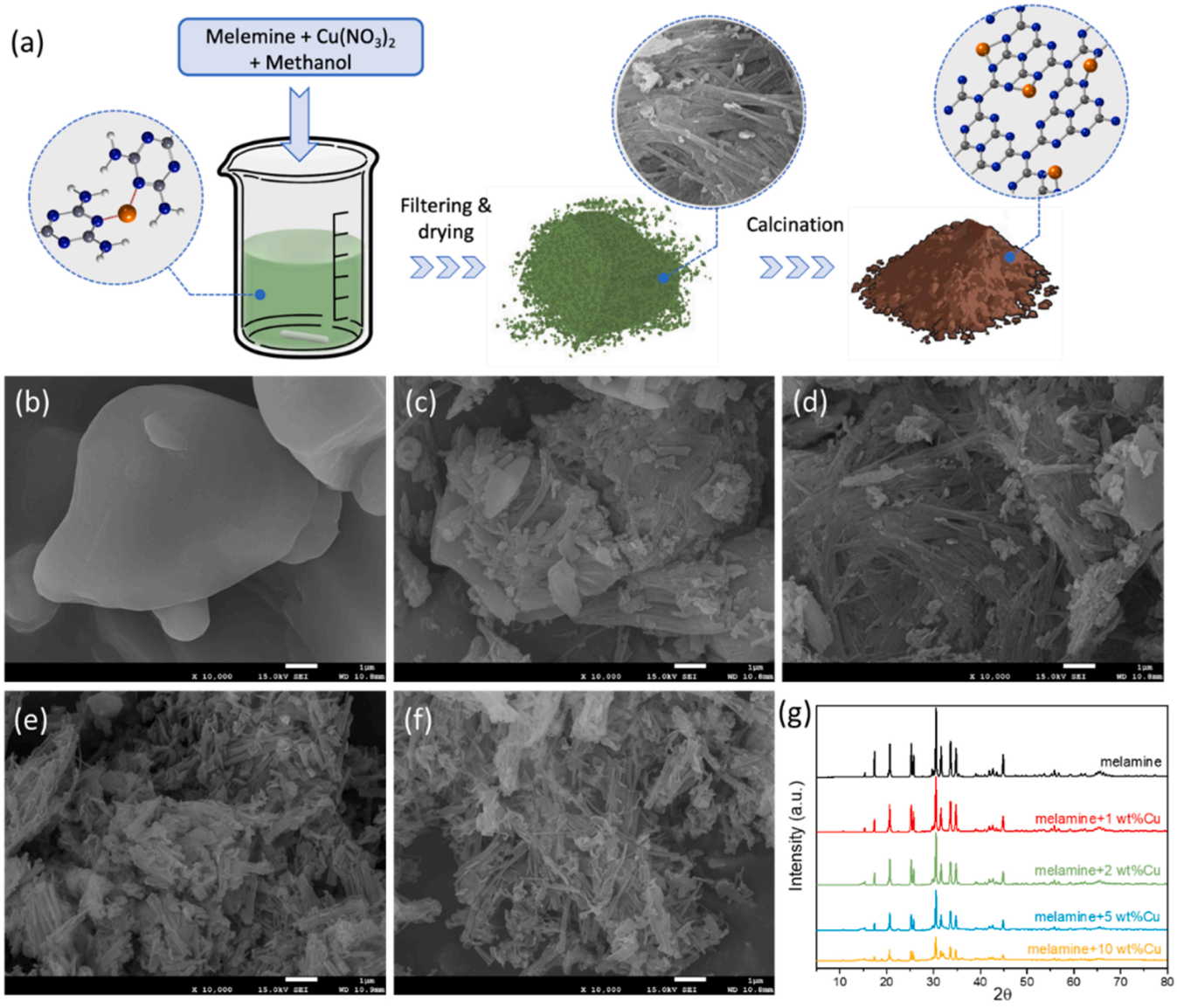

Fig. 1. (a) Schematic illustration of the preparation process of CN-xCu samples. Scanning electron microscope (SEM) images of the morphology of (b) pristine melamine and melamine-$Cu(NO_3)_2$ complex with (c) 1 wt%, (d) 2 wt%, (e) 5 wt%, (f) 10 wt% Cu in mass ratio. (g) corresponding XRD patterns of the samples.

performed X-ray photoelectron spectroscopy (XPS) measurement on a typical sample (CN-2Cu). The spectrum recorded on the Cu 2p shows two sharp peaks corresponding to $2p_{1/2}$ and $2p_{3/2}$, respectively, without obvious shake-up signals in between, indicating that the Cu species is not in bivalent (Fig. S5) [38,39]. However, it is difficult to further differentiate Cu^0 and Cu^I species based on Cu 2p because of the high similarity of the two spectra. Therefore, we turned to study the Cu LMM spectrum of the sample and compare the results with various Cu references in Wagner plot which is based on the Auger parameter, therefore being able to eliminate the surface-charging effect of samples and display a more obvious chemical shift [38,40–42]. As shown in Fig. 4, the Cu species in CN shows an Auger parameter of 1847.6 eV, having a 0.4–3 eV difference with that of metallic copper, copper oxide, copper hydroxide, and copper halides, but very close to that of CuCN in which Cu is coordinated with C and N, respectively, suggesting the Cu atoms most likely have a valence of $+1$ and there should be a chemical bonding between atomically dispersed Cu and the CN framework.

The coordination environment of Cu atoms in CN-xCu was investigated by synchrotron-based X-ray absorption spectroscopy (XAS) and X-ray photoelectron spectroscopy (XPS). As revealed by the Cu K-edge of X-ray absorption near edge structure (XANES) spectra (Fig. 5a), the sample CN-2Cu has an absorption edge sitting between those for Cu foil and CuO reference samples, signalling the existence of Cu^+ as the predominant oxidation state [41]. This result is in line with the XPS analysis. The atomical dispersion of Cu species was further confirmed by the Fourier transformed k^3-weighted Cu K-edge EXAFS spectra (Fig. 5b). The absence of the peak at ~2.2 Å which corresponds to metallic Cu-Cu bond confirms the single-atom nature of Cu, consistent with that from HAADF-STEM. The CN-2Cu sample exhibits a major peak at ~1.5 Å which can be ascribed to the Cu–N bond [22,43]. Wavelet transform analysis was performed to further validate the Cu-N coordination. Compared to CuO (Fig. 5d), the Cu atoms in CN-2Cu (Fig. 5c) have a shorter coordination bond length (the vertical axis, c.a. 1.4 Å) and coordinate with lighter atoms than O (the smaller the horizontal axis value, the lighter the coordination atoms, in this case 5.5 $Å^{-1}$ vs. 6.5 $Å^{-1}$), confirming the Cu-N coordination.

More information about the coordination environment of Cu atoms in CN-xCu can be inferred by the Cu K-edge XANES (Fig. 5a). According to the calculation results reported by literature, the broad peaks at around 8995.0 eV and 9003.7 eV imply that there could be two types of

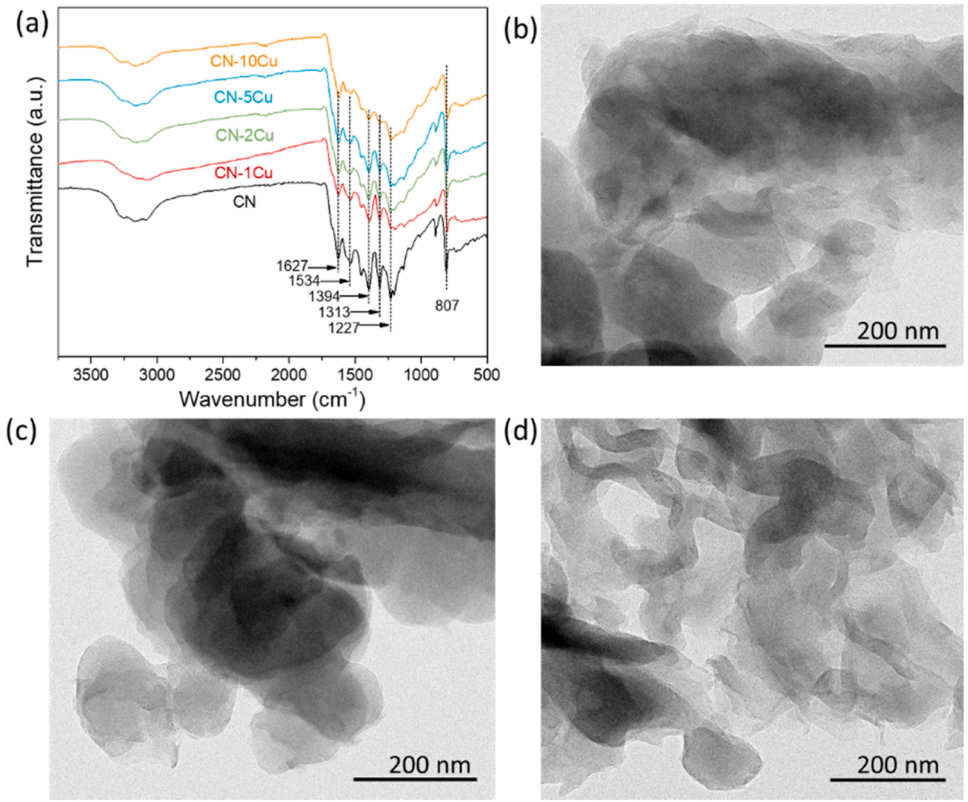

Fig. 2. (a) FTIR spectra of samples. HRTEM images of (b) CN, (c) CN-2Cu, and (d) CN-5Cu.

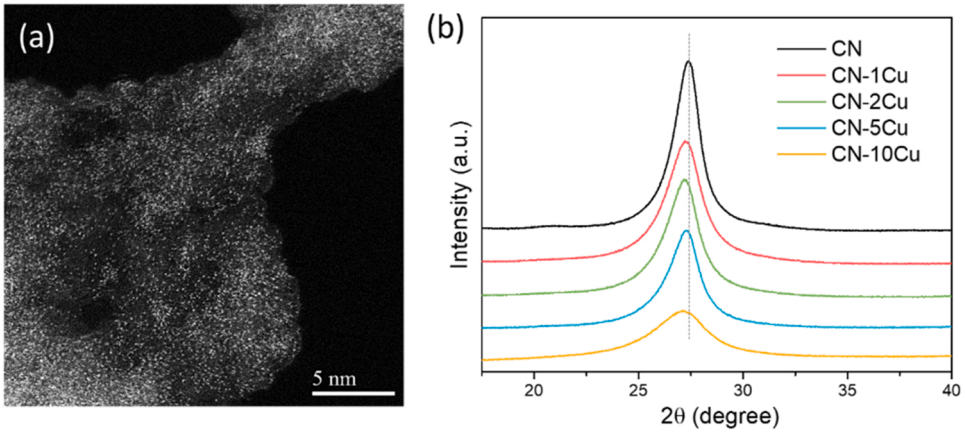

Fig. 3. (a) Representative High-angle annular dark-field scanning transmission electron microscopy (HAADF-STEM) image of CN-2Cu. (b) XRD patterns of Cu-incorporated CN samples.

coordination environment for Cu atoms, namely the Cu-N_3 (intralayer) and Cu-N_4 (interlayer) manners [22]. More direct evidence of the configuration is given by the Cu K-edge fitting results that show a Cu coordination number of 3.47, indicating the coexistence of the two manners (Fig. S6, Table S1). Since there are three types of N in the CN framework (inset in Fig. 5e), the pyridinic nitrogen (C-N═C), the central nitrogen singly bonded to three carbons N-$(C)_3$, and the nitrogen in amino groups (C-N-H), we carefully studied the high-resolution N 1 s XPS spectra of samples to identify coordination sites with Cu atoms [44, 45]. As shown in Fig. 5e, the N1s core level spectra can be deconvoluted with three Voigt components corresponding to three distinct nitrogen sites in CN. In CN-xCu samples, the pyridinic nitrogen shows a 0.1–0.3 eV shift toward low binding energy, while binding energies for the other two types of nitrogen almost keep unchanged in different samples, strongly evidencing a chemical bonding between Cu atoms and pyridinic nitrogen. Moreover, the effect of Cu-incorporation to the CN framework is reflected by the peak at 807 cm^{-1} in FTIR spectra that can be ascribed to the breathing vibration of the tri-s-triazine structure of graphitic carbon nitride [15,46]. The peak showed a red-shift in CN-xCu samples, suggesting a decreased vibration frequency due to coordination (Fig. S7).

3.3. *Electronic structure of the CN-xCu supports*

To study the change of electronic structures upon Cu incorporation, the valence band spectra of samples were collected by XPS. As displayed in Fig. 6a, the peaks associated with valence bands increase significantly as the Cu content, with the onset of the valence band gradually shifting

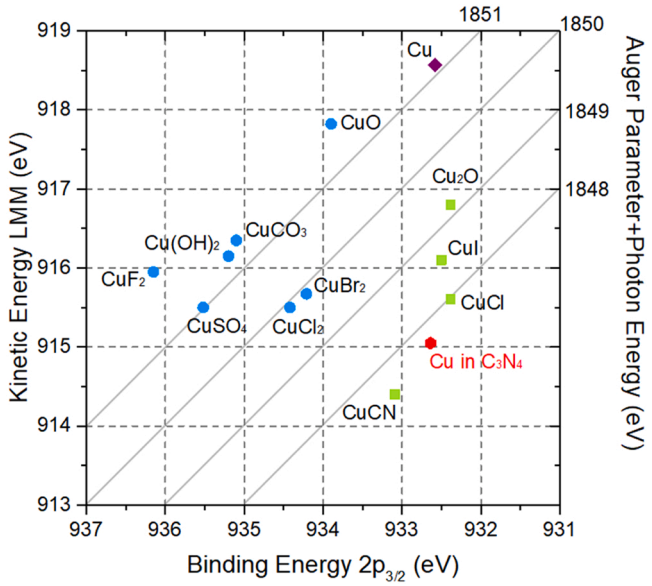

Fig. 4. Cu Wagner plot of CN-2Cu with metallic Cu and several typical Cu(I) and Cu (II) compounds as reference; Data from NIST X-ray Photoelectron Spectroscopy Database, Version 4.1 (accessed Oct. 2021).

toward lower binding energy side, suggesting that the valence band moves toward Fermi levels. For CN-10Cu, the shift is as high as 1.12 eV. It is well documented that the valence band of carbon nitride mainly consists of the 2p orbitals of sp^2 nitrogen on the heptazine ring, with less contribution from 2p orbitals of carbon atoms and nitrogen atoms of amino groups [45]. Therefore, the increased valence band peak can be ascribed to the electron drift from Cu to N atoms, which led to the formation of Cu^+ species and electron-rich nitrogen in the CN framework, and consequently lifted the valence band top.

The bandgaps were determined by Tauc plot (Fig. 6b) that derived from the UV-Vis absorption spectra of samples. For pristine CN, the bandgap was measured to be 2.56 eV, close to the values reported in the literatures [47–49]. After introducing 2 wt% of Cu atoms, the bandgap shrank to 2.02 eV. Further increasing the Cu content resulted in a continuous narrowing of bandgaps, achieving a minimum of 1.86 eV in CN-10Cu. The corresponding conduction band bottom of samples were calculated according to their valence band top and bandgaps. The resulted energy-band structure chart (Fig. S9) of samples showed that the narrowed bandgap mainly resulted from elevated valence band while the conduction band shifted marginally.

The work functions of CN-xCu samples were determined using the secondary electron cut-off (SECO) by ultraviolet photoelectron spectroscopy (UPS). As shown in Fig. 6c, the pristine CN has a work function of 4.43 eV and the value reduces to 4.08 and 4.03 eV for CN-2Cu and CN-5Cu, respectively, illustrating an escalating trend of Fermi level of samples. Since electron transfer between semiconductor supports and metal nanoparticles could occur after they electronically contact with each other and this process is mainly driven by the work function difference of the two [50], lower work function values suggest stronger electron-donating tendency and therefore are expected to have profound electronic effect to their supported metal nanoparticles.

3.4. Support effect for enhanced photocatalytic Suzuki cross-coupling

We deposited Pd nanoparticles onto the CN-xCu surface and investigated how these Cu atoms affect the activity of Pd toward photocatalytic Suzuki cross-coupling reactions [51]. The Pd loading was fixed at 2 wt% for all the catalysts used in this work, noted as Pd/CN-xCu. As shown in the HAADF-STEM image (Fig. 7a), the light spots indicate that Pd nanoparticles were evenly dispersed on the CN-2Cu support, with an average size around 3 nm. Apart from the surface Pd nanoparticles, these confluent light dots resulted from Cu atoms in the CN framework

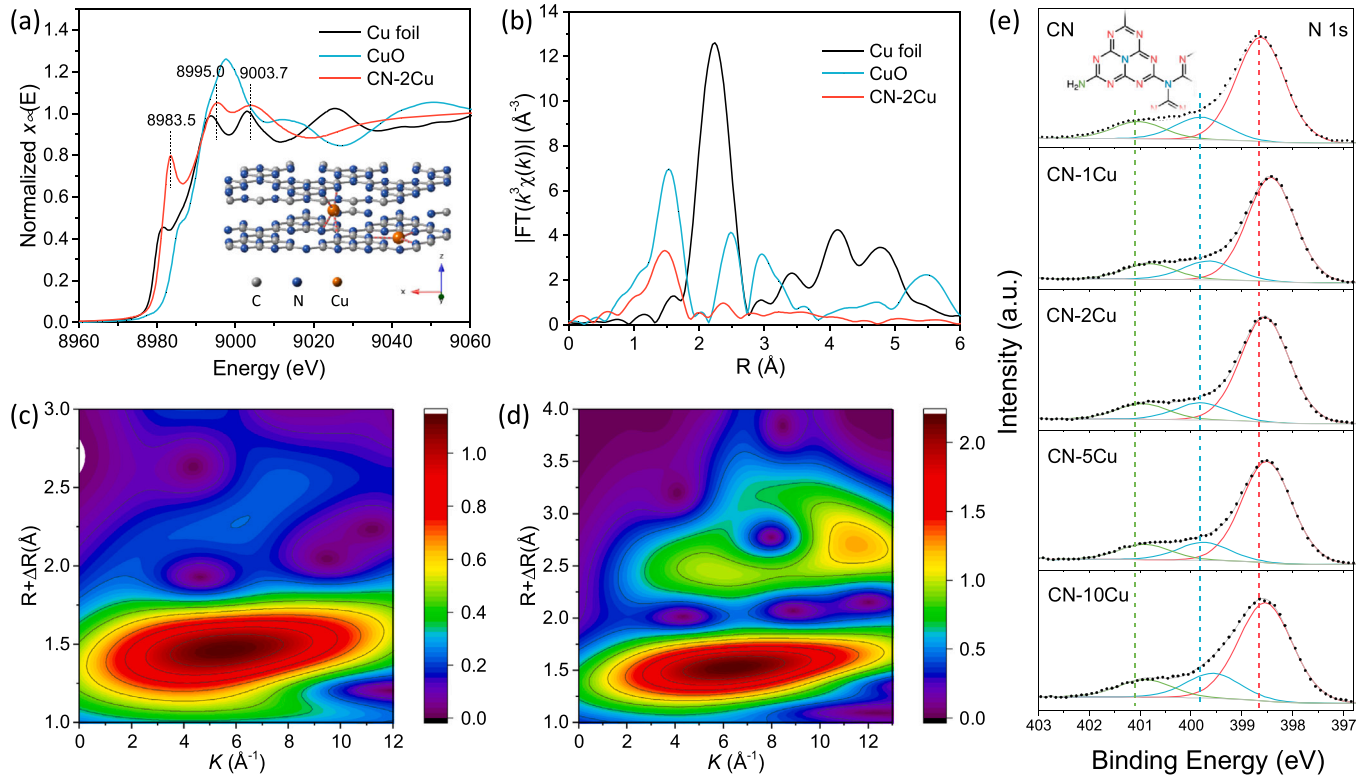

Fig. 5. (a) Cu K-edge XANES spectra of CN-2Cu, CuO and Cu foil. (b) Fourier transformed magnitude of the experimental Cu K-edge extended X-ray absorption fine structure (EXAFS) signal of CN-2Cu, CuO, and Cu foil. Wavelet transform (WT) of (c) CN-2Cu and (d) CuO. (e) N1s core level XPS spectra of samples.

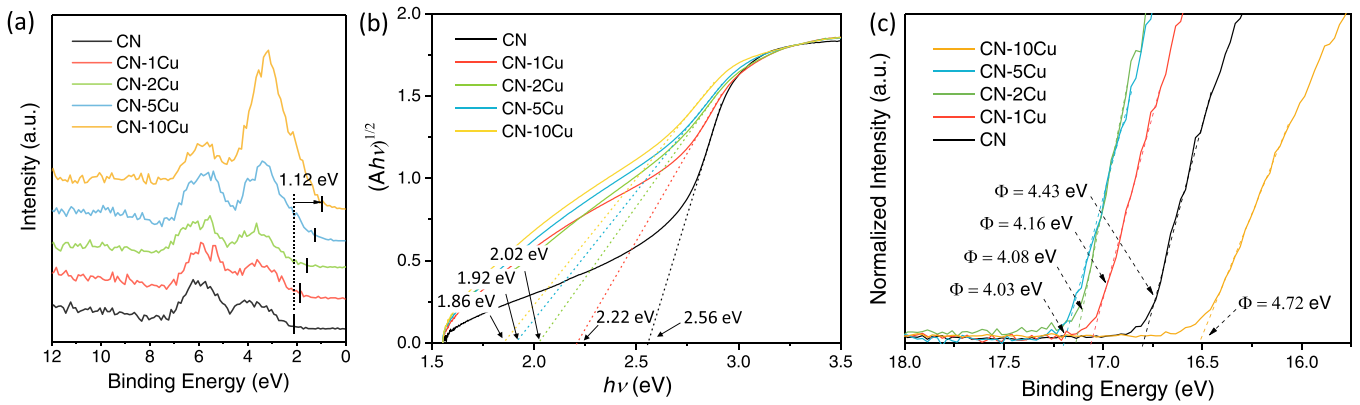

Fig. 6. (a) Valence band spectra of samples collected under XPS mode. (b) Tauc plot of samples transformed from the UV-Vis absorption spectra shown in Fig. S8. (c) UPS spectra of samples.

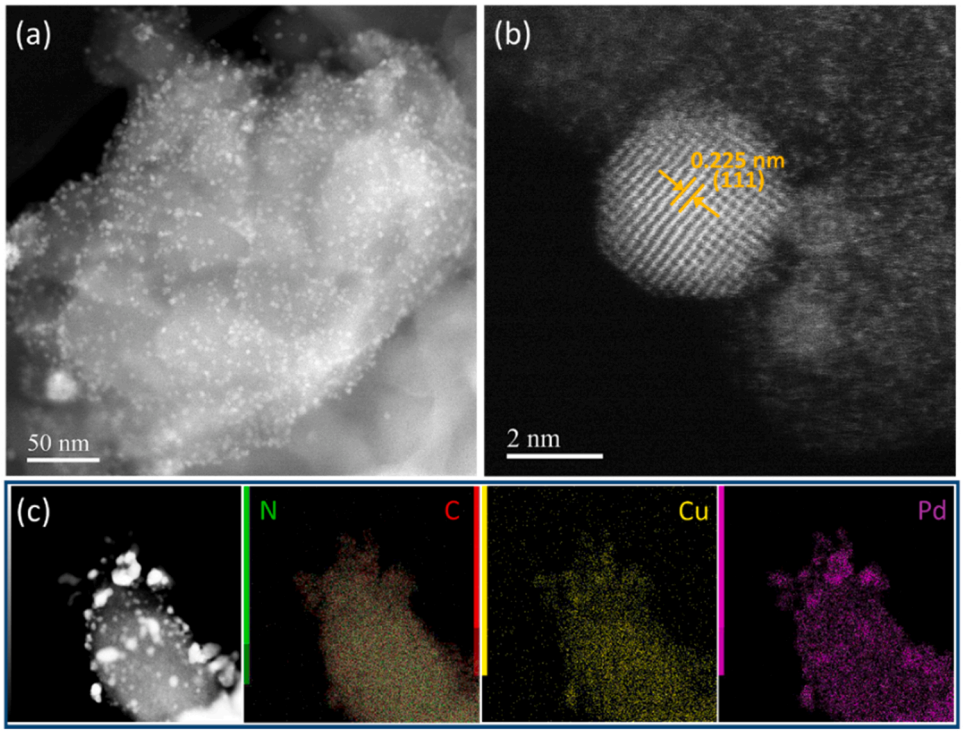

Fig. 7. (a, b) HAADF-STEM images and (c) STEM EDS mapping on a selected area of Pd/CN-2Cu. The mapping results for C and N elements were technically processed to overlap.

underneath, which was further confirmed by the locally enlarged image (Fig. 7b). The fringe spacing of an isolated Pd nanoparticle was measured to be 0.225 nm, corresponding to the (111) planes of face-centred cubic palladium. The energy-dispersive X-ray spectroscopy (EDS) mapping on a selected area (Fig. 7c) displays the elemental distribution of the sample, showing results in line with the observation in HAADF-STEM images.

Next, phenylboronic acid and 4-iodotoluene were employed as two substrates for the cross-coupling reaction under visible light irradiation over the Pd/Cu-xCN catalyst (Fig. 8a); K_3PO_4 was selected as a base additive after screening (Fig. S10). In a control experiment, the CN-2Cu support alone did not give any product, excluding the direct catalytic contribution from the support. Nevertheless, the support showed strong effect on the catalytic activity of the loaded Pd nanoparticles. As a baseline, 28 % yield of 4-phenyltoluene was obtained over the Pd/CN catalyst in dark, and the yield doubled with light irradiation. After Cu-incorporation, the catalytic activity in dark was improved by 10–15 % and the improvement was greatly enlarged under light irradiation. For the optimal catalyst Pd/CN-2Cu, 98 % 4-phenyltoluene yield was obtained after 50 min of light reaction, corresponding to a turnover frequency (TOF) of 62.3 h^{-1} (Table S2). The light-resulted enhancement exhibited a proportional relationship to the light intensity (Fig. S11). For other catalysts with 1, 5, and 10 wt% of Cu contents, the catalytic activities were all lower than that of CN-2Cu, corroborating the fact that Cu-incorporation leads to the activity change of Pd nanoparticles.

In the action spectrum of the Pd/CN-2Cu catalyst (Fig. 8b), i.e. apparent quantum efficiency as a function of excitation wavelength, higher AQEs were observed at lower wavelengths, with approximately 19% AQE achieved under 420 nm light illumination. Notably, the AQEs matched well with the absorption spectrum of CN-2Cu, rather than the pristine CN, confirming the contribution of Cu-resulted-light-absorption-enhancement to the reaction. Since photogenerated holes are essential for activating arylboronic acids in Suzuki cross-coupling reactions by cleaving the C-B bonds [33], the enhanced

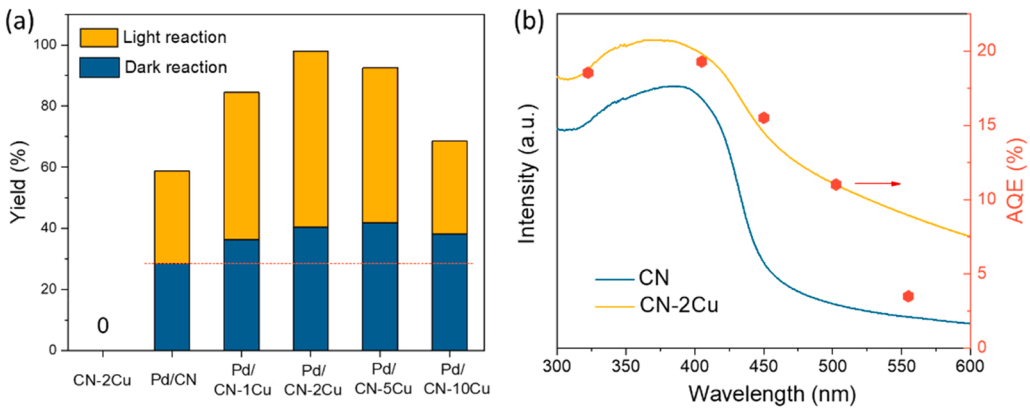

Fig. 8. (a) The catalytic activity of the Pd/CN-xCu catalysts on Suzuki cross-coupling reactions. Reaction conditions: 10 mg catalysts; 0.1 mmol (1 equiv.) 4-iodotoluene; 1.2 equiv. phenylboronic acid; 3 equiv. K_3PO_4; 2 mL EtOH/H_2O (2:1) as solvent; N_2 atmosphere; 25 °C; 420 nm light; 100 mW/cm^2 light intensity; 50 min (b) Action spectrum of the optimum catalyst, Pd/CN-2Cu. Apparent quantum efficiency (AQE) was calculated based on the light contribution (the conversion under light subtracts the conversion in dark) under each wavelength at low conversion (below 50%) and the assumption that producing 1 mol of product consumes 1 mol of photogenerated holes [33]. The light intensity for each wavelength was fixed at 15 mW/cm^2. The absorption spectrum of the pristine CN is also presented for reference.

light-absorption and improved intralayer/interlayer carrier transfer originated from Cu-incorporation would be kinetically beneficial to the increase of surface carriers and therefore promotes the reaction.

3.5. Step-by-step insights into the reaction mechanism

The interaction between supports and Pd nanoparticles through electronic effect played a critical role in the reaction. As metallic Pd has a work function of 5.22 eV, much higher than that of CN-xCu (Fig. 6c), electron transfer from the support to Pd nanoparticles occurs until the two Fermi levels are aligned and meanwhile Schottky barriers were formed at the semiconductor-metal interface (Fig. 9) [50,52]. Therefore, the lower work function of CN-2Cu led to more electron-rich Pd surfaces compared to Pd/CN, which was also reflected by the fact that CN-xCu supported Pd nanoparticles were more easily to be oxidized in air. Table S3 gave the relative ratio of $Pd^{(0)}$, $Pd^{(II)}$, and $Pd^{(IV)}$ in different samples stored in air for one week. Pd/CN had the highest ratio of metallic Pd species, whereas the ratio of $Pd^{(0)}$ in Pd/CN-xCu gradually decreased with the increase of Cu content (oxidized Pd species increased correspondingly).

To investigate how the electron-rich Pd surface affects the reaction, we monitored the catalytic activity of Pd/CN-2Cu in each elementary step of the cross-coupling reaction. As a general recognition, the Suzuki cross-coupling reaction mainly involves three elementary steps: oxidative addition, transmetalation, and reductive elimination, where oxidative addition is also identified as the rate-determining step of the overall reaction (Fig. 10a) [53,54]. Since oxidative addition occurs between aryl halides and $Pd^{(0)}$ (see the reaction equation in Fig. 10b), it can be considered as a chemical adsorption process. Therefore, the reaction rate of the oxidative addition step can be reflected by the concentration change of 4-iodotoluene in the absence of phenylboronic acid. As shown in Fig. 10b, with Pd/CN-2Cu as the catalyst, the concentration of 4-iodotoluene showed a decrease more evident that than of using Pd/CN as the catalyst, especially in the first two minutes, suggesting that the oxidative addition step proceeded much faster on Pd/CN-2Cu. We ascribed this enhancement in reaction rate to the more electron-rich Pd surface of Pd/CN-2Cu, where an easier electron injection from $Pd^{(0)}$ to the lowest unoccupied molecular orbital (LUMO) of 4-iodotoluene would be allowed. Such a tendency would benefit the C-I bond cleavage and the generation of the adduct intermediate (1), namely the 4-iodotoluene-chemisorbed catalyst.

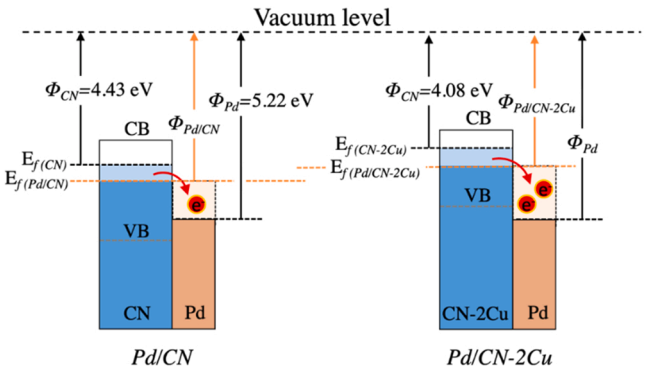

Fig. 9. Schematic illustration of the electron transfer from support to Pd nanoparticles.

In the next step, intermediate (1) was collected by filtration and redispersed in a K_3PO_4 solution to produce intermediate (2) through substituting adsorbed -I by -PO_4^{3-} (Fig. 10c). Meanwhile, phenylboronic acid and K_3PO_4 were premixed in another vial to generate intermediate (3). Afterwards, the two solutions were mixed to produce intermediate (4). During this process, the consumption of intermediate (3) was monitored (see Fig. S12 for quantitative method) and regarded as the reaction rate of the transmetalation step while the final coupling product (5) was quantified at the same time. Although the generation rate of the coupling product did not equal the reaction rate of the reductive elimination step, it provided information on the total reaction rate of last two elementary steps (measurement of the isolated reductive elimination rate is challenging because it consecutively occurs after the transmetalation step). As shown in Fig. 10c, the transmetalation on Pd/CN-2Cu seems still faster than that on Pd/CN, but the difference was significantly narrowed compared to that for the oxidative addition step. Moreover, the coupling product was first detected for Pd/CN-2Cu at 30 s, suggesting an overall faster reaction rate of the transmetalation and reductive elimination steps (Fig. 10d). Nevertheless, we tend to ascribe the improved catalytic activity to the promotion of rate-determining step (oxidative addition) by the electron-rich Pd surface that resulted from the electronic effect of Cu-incorporated CN supports. For non-rate-determining steps (transmetalation and reductive elimination), although their rates were also affected by different catalysts, they may have negligible influence on the overall reaction rate considering that they proceed much faster than the rate-determining step.

4. Conclusions

In conclusion, we present in this work the non-catalytic single-atom Cu species in the bulk of carbon nitride promotes the activity of the surface Pd nanoparticles through enhanced support effect. HAADF-STEM, XAFS, and XPS results showed that Cu species is in + 1 oxidation state and atomically coordinates with the pyridinic nitrogen. The

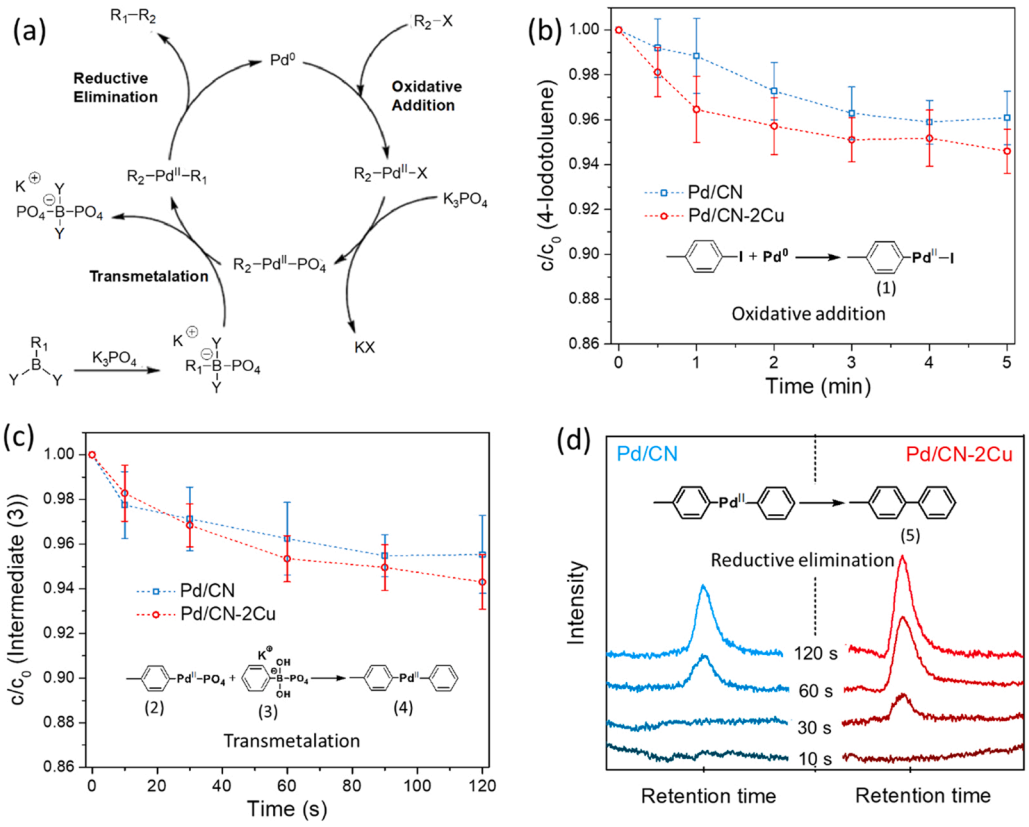

Fig. 10. (a) Generally recognized three elementary steps in Suzuki cross-coupling reactions. (b) 4-iodotoluene concentration change in the oxidative addition step. 500 mg of the catalyst and 10 mL of 1 mM 4-iodotoluene were used for this experiment. (c) The concentration change of intermediate (3) in the transmetalation step. For the generation of intermediate (2), 500 mg of the catalyst and 10 mL of 1 M 4-iodotoluene were used for pre-adsorption and the mixture was stirred overnight to reach adsorption equilibrium. Afterwards, the resulting solid was redispersed in 10 mL of 0.1 M K_3PO_4 solution and collected after 2 h. (d) Gas chromatograph spectra of the coupling product obtained after the reductive elimination step.

CN-xCu support showed elevated valance bands, lower work functions, and narrower bandgaps as compared to the pristine CN, due to the electron drift from Cu to N. As a result, the CN-xCu support enhanced the photocatalytic activity of Pd nanoparticles in Suzuki cross-coupling reactions, which can be partially ascribed to the improved proton harvesting and more effective carrier transfer promoted by interlayer Cu species. A more critical role was the enhanced electronic effect of CN-Cu to the surface Pd resulted from Cu-incorporation, which leading to an electron-rich Pd surface. Such Pd surfaces promoted the electron injection from $Pd^{(0)}$ to the lowest unoccupied molecular orbital (LUMO) of 4-iodotoluene and thereby benefited the cleavage of the C-I bond in the coupling reaction. As a result, the oxidative addition step, namely the rate-determining step of the coupling reaction, was significantly accelerated, which is responsible to the overall catalytic activity improvement. This study will provide useful insights for improving the catalytic activity by well regulating and designing the electronic structure of the support material via single atom modulation.

CRediT authorship contribution statement

Chenhui Han: Conceptualization, Investigation, Writing – original draft. **Ruijuan Qi:** Investigation, Resources. **Ruolun Sun:** Investigation. **Kaicai Fan:** Formal analysis. **Bernt Johannessen:** Formal analysis. **Dong-Chen Qi:** Formal analysis, Resources. **Shaowen Cao:** Writing – review & editing. **Jingsan Xu:** Conceptualization, Supervision, Writing – review & editing, Funding acquisition.

Declaration of Competing Interest

The authors declare that they have no known competing financial interests or personal relationships that could have appeared to influence the work reported in this paper.

Data Availability

Data will be made available on request.

Acknowledgements

J.X. and D.C.Q. are grateful for the financial support of Australia Research Council (DP190101607). We thank the Central Analytical Research Facility (CARF) at QUT for technical assistance.

Appendix A. Supporting information

Supplementary data associated with this article can be found in the online version at doi:10.1016/j.apcatb.2022.121954.

References

[1] I.C. Gerber, P. Serp, A theory/experience description of support effects in carbon-supported catalysts, Chem. Rev. 120 (2020) 1250–1349.
[2] M. Comotti, W.-C. Li, B. Spliethoff, F. Schüth, Support effect in high activity gold catalysts for CO oxidation, J. Am. Chem. Soc. 128 (2006) 917–924.
[3] L.J. Burcham, I.E. Wachs, The origin of the support effect in supported metal oxide catalysts: In situ infrared and kinetic studies during methanol oxidation, Catal. Today 49 (1999) 467–484.
[4] N.B. Van, D. Laurenti, P. Delichère, C. Geantet, Hydrodeoxygenation of guaiacol part II: Support effect for CoMoS catalysts on HDO activity and selectivity, Appl. Catal. B 101 (2011) 246–255.
[5] X.Y. Liu, A. Wang, T. Zhang, C.-Y. Mou, Catalysis by gold: new insights into the support effect, Nano Today 8 (2013) 403–416.
[6] X. Zhang, R. Sa, S. Yang, F. Zhou, Z. Jiang, R. Wang, A non-carbon catalyst support upgrades the intrinsic activity of ruthenium for hydrogen evolution electrocatalysis via strong interfacial electronic effects, Nano Energy 75 (2020), 104981.
[7] A.A. Pollit, S. Ye, D.S. Seferos, Elucidating the role of catalyst steric and electronic effects in controlling the synthesis of π-conjugated polymers, Macromolecules 53 (2020) 138–148.
[8] B. Coq, F. Figueras, Bimetallic palladium catalysts: Influence of the co-metal on the catalyst performance, J. Mol. Catal. A: Chem. 173 (2001) 117–134.

[9] X. Wang, K. Maeda, A. Thomas, K. Takanabe, G. Xin, J.M. Carlsson, K. Domen, M. Antonietti, A metal-free polymeric photocatalyst for hydrogen production from water under visible light, Nat. Mater. 8 (2009) 76–80.

[10] Y. Zhao, M. Antonietti, Visible-light-irradiated graphitic carbon nitride photocatalyzed Diels-Alder reactions with dioxygen as sustainable mediator for photoinduced electrons, Angew. Chem. Int. Ed. Engl. 56 (2017) 9336–9340.

[11] Y. Dai, C. Li, Y. Shen, T. Lim, J. Xu, Y. Li, H. Niemantsverdriet, F. Besenbacher, N. Lock, R. Su, Light-tuned selective photosynthesis of azo-and azoxy-aromatics using graphitic C_3N_4, Nat. Commun. 9 (2018) 1–7.

[12] C. Han, P. Meng, E.R. Waclawik, C. Zhang, X.H. Li, H. Yang, M. Antonietti, J. Xu, Palladium/graphitic carbon nitride (g-C_3N_4) stabilized emulsion microreactor as a store for hydrogen from ammonia borane for use in alkene hydrogenation, Angew. Chem. Int. Ed. 57 (2018) 14857–14861.

[13] Z. Chen, E. Vorobyeva, S. Mitchell, E. Fako, M.A. Ortuño, N. López, S.M. Collins, P. A. Midgley, S. Richard, G. Vilé, A heterogeneous single-atom palladium catalyst surpassing homogeneous systems for suzuki coupling, Nat. Nanotechnol. 13 (2018) 702.

[14] S. Yang, Y. Gong, J. Zhang, L. Zhan, L. Ma, Z. Fang, R. Vajtai, X. Wang, P. M. Ajayan, Exfoliated graphitic carbon nitride nanosheets as efficient catalysts for hydrogen evolution under visible light, Adv. Mater. 25 (2013) 2452–2456.

[15] J. Zhang, X. Chen, K. Takanabe, K. Maeda, K. Domen, J.D. Epping, X. Fu, M. Antonietti, X. Wang, Synthesis of a carbon nitride structure for visible-light catalysis by copolymerization, Angew. Chem. Int. Ed. 49 (2010) 441–444.

[16] C. Han, L. Du, M. Konarova, D.-C. Qi, D.L. Phillips, J. Xu, Beyond hydrogen evolution: Solar-driven, water-donating transfer hydrogenation over platinum/carbon nitride, ACS Catal. 10 (2020) 9227–9235.

[17] Z. Chen, S. Mitchell, E. Vorobyeva, R.K. Leary, R. Hauert, T. Furnival, Q. M. Ramasse, J.M. Thomas, P.A. Midgley, D. Dontsova, M. Antonietti, S. Pogodin, N. López, J. Pérez-Ramírez, Stabilization of single metal atoms on graphitic carbon nitride, Adv. Funct. Mater. 27 (2017), 1605785.

[18] Q. Jia, S. Zhang, X. Jia, X. Dong, Z. Gao, Q. Gu, Photocatalytic coupled redox cycle for two organic transformations over Pd/carbon nitride composites, Catal. Sci. Technol. 9 (2019) 5077–5089.

[19] X. Jia, J. Zhao, Y. Lv, X. Fu, Y. Jian, W. Zhang, Y. Wang, H. Sun, X. Wang, J. Long, Low-crystalline PdCu alloy on large-area ultrathin 2D carbon nitride nanosheets for efficient photocatalytic Suzuki coupling, Appl. Catal. B 300 (2022), 120756.

[20] Z. Zeng, Y. Su, X. Quan, W. Choi, G. Zhang, N. Liu, B. Kim, S. Chen, H. Yu, S. Zhang, Single-atom platinum confined by the interlayer nanospace of carbon nitride for efficient photocatalytic hydrogen evolution, Nano Energy 69 (2020), 104409.

[21] Y. Xiong, W. Sun, P. Xin, W. Chen, X. Zheng, W. Yan, L. Zheng, J. Dong, J. Zhang, D. Wang, Gram-scale synthesis of high-loading single-atomic-site Fe catalysts for effective epoxidation of styrene, Adv. Mater. (2020), 2000896.

[22] X. Xiao, Y. Gao, L. Zhang, J. Zhang, Q. Zhang, Q. Li, H. Bao, J. Zhou, S. Miao, N. Chen, A promoted charge separation/transfer system from Cu single atoms and C_3N_4 layers for efficient photocatalysis, Adv. Mater. (2020), 2003082.

[23] L. Li, D. Cruz, A. Savateev, G. Zhang, M. Antonietti, Y. Zhao, Photocatalytic cyanation of carbon nitride scaffolds: Tuning band structure and enhancing the performance in green light driven CS bond formation, Appl. Catal. B 229 (2018) 249–253.

[24] M. Shalom, M. Guttentag, C. Fettkenhauer, S. Inal, D. Neher, A. Llobet, M. Antonietti, In situ formation of heterojunctions in modified graphitic carbon nitride: Synthesis and noble metal free photocatalysis, Chem. Mater. 26 (2014) 5812–5818.

[25] S. An, G. Zhang, T. Wang, W. Zhang, K. Li, C. Song, J.T. Miller, S. Miao, J. Wang, X. Guo, High-density ultra-small clusters and single-atom Fe sites embedded in graphitic carbon nitride (g-C_3N_4) for highly efficient catalytic advanced oxidation processes, ACS Nano 12 (2018) 9441–9450.

[26] L. Zhang, R. Long, Y. Zhang, D. Duan, Y. Xiong, Y. Zhang, Y. Bi, Direct observation of dynamic bond evolution in single-atom Pt/C_3N_4 catalysts, Angew. Chem. Int. Ed. 59 (2020) 6224–6229.

[27] A.M. Abdel-Mageed, B. Rungtaweevoranit, M. Parlinska-Wojtan, X. Pei, O. M. Yaghi, R.Jr Behm, Highly active and stable single-atom Cu catalysts supported by a metal–organic framework, J. Am. Chem. Soc. 141 (2019) 5201–5210.

[28] B.-H. Lee, S. Park, M. Kim, A.K. Sinha, S.C. Lee, E. Jung, W.J. Chang, K.-S. Lee, J. H. Kim, S.-P. Cho, Reversible and cooperative photoactivation of single-atom Cu/TiO_2 photocatalysts, Nat. Mater. 18 (2019) 620–626.

[29] N. Zhang, C. Ye, H. Yan, L. Li, H. He, D. Wang, Y. Li, Single-atom site catalysts for environmental catalysis, Nano Res. 13 (2020) 3165–3182.

[30] T. Zhu, Q. Chen, P. Liao, W. Duan, S. Liang, Z. Yan, C. Feng, Single-atom Cu catalysts for enhanced electrocatalytic nitrate reduction with significant alleviation of nitrite production, Small 16 (2020), 2004526.

[31] C. Xu, X. Zhi, A. Vasileff, D. Wang, B. Jin, Y. Jiao, Y. Zheng, S.-Z. Qiao, Highly selective two-electron electrocatalytic CO_2 reduction on single-atom Cu catalysts, Small Struct. 2 (2021), 2000058.

[32] J. Büker, X. Huang, J. Bitzer, W. Kleist, M. Muhler, B. Peng, Synthesis of Cu single atoms supported on mesoporous graphitic carbon nitride and their application in liquid-phase aerobic oxidation of cyclohexene, ACS Catal. 11 (2021) 7863–7875.

[33] X.-H. Li, M. Baar, S. Blechert, M. Antonietti, Facilitating room-temperature Suzuki coupling reaction with light: Mott-schottky photocatalyst for C-C-coupling, Sci. Rep. 3 (2013) 1743.

[34] E. Kroke, M. Schwarz, E. Horath-Bordon, P. Kroll, B. Noll, A.D. Norman, Tri-s-triazine derivatives. Part I. From trichloro-tri-s-triazine to graphitic C_3N_4 structures, New J. Chem. 26 (2002) 508–512.

[35] J. Wei, P. Hing, Z.Q. Mo, Tem, XPS and FTIR characterization of sputtered carbon nitride films, Surf. Interface Anal. 28 (1999) 208–211.

[36] J. Xu, H. Wang, C. Zhang, X. Yang, S. Cao, J. Yu, M. Shalom, From millimeter to subnanometer: vapor–solid deposition of carbon nitride hierarchical nanostructures directed by supramolecular assembly, Angew. Chem. Int. Ed. 29 (2017) 8426–8430.

[37] H.E. Kim, I.H. Lee, J. Cho, S. Shin, H.C. Ham, J.Y. Kim, H. Lee, Palladium single-atom catalysts supported on C@C_3N_4 for electrochemical reactions, ChemElectroChem 6 (2019) 4757–4764.

[38] G. Moretti, A. Palma, E. Paparazzo, M. Satta, Auger parameter and wagner plot studies of small copper clusters, Surf. Sci. 646 (2016) 298–305.

[39] M.C. Biesinger, Advanced analysis of copper X-ray photoelectron spectra, Surf. Interface Anal. 49 (2017) 1325–1334.

[40] G. Moretti, F. Filippone, M. Satta, Use of auger parameter and wagner plot in the characterization of Cu-ZSM-5 catalysts, Interfaces Thin Films 31 (2001) 249–254.

[41] S. Velu, K. Suzuki, C.S. Gopinath, H. Yoshida, T. Hattori, XPS, XANES and EXAFS investigations of CuO/ZnO/Al_2O_3/ZrO_2 mixed oxide catalysts, Phys. Chem. Chem. Phys. 4 (2002) 1990–1999.

[42] G. Moretti, Auger parameter and wagner plot in the characterization of chemical states: initial and final state effects, J. Electron. Spectrosc. Relat. Phenom. 76 (1995) 365–370.

[43] L. Zong, K. Fan, W. Wu, L. Cui, L. Zhang, B. Johannessen, D. Qi, H. Yin, Y. Wang, P. Liu, Anchoring single copper atoms to microporous carbon spheres as high-performance electrocatalyst for oxygen reduction reaction, Adv. Funct. Mater. 31 (2021), 2104864.

[44] A.P. Dementjev, A. De Graaf, M.C.M. Van de Sanden, K.I. Maslakov, A.V. Naumkin, A.A. Serov, X-ray photoelectron spectroscopy reference data for identification of the C_3N_4 phase in carbon–nitrogen films, Diam. Relat. Mater. 9 (2000) 1904–1907.

[45] K. Akaike, K. Aoyama, S. Dekubo, A. Onishi, K. Kanai, Characterizing electronic structure near the energy gap of graphitic carbon nitride based on rational interpretation of chemical analysis, Chem. Mater. 30 (2018) 2341–2352.

[46] J. Fu, B. Zhu, C. Jiang, B. Cheng, W. You, J. Yu, Hierarchical porous O-doped g-C_3N_4 with enhanced photocatalytic CO_2 reduction activity, Small 13 (2017), 1603938.

[47] Y. Zheng, L. Lin, B. Wang, X. Wang, Graphitic carbon nitride polymers toward sustainable photoredox catalysis, Angew. Chem. Int. Ed. 54 (2015) 12868–12884.

[48] L. Jiang, X. Yuan, Y. Pan, J. Liang, G. Zeng, Z. Wu, H. Wang, Doping of graphitic carbon nitride for photocatalysis: a reveiw, Appl. Catal. B 217 (2017) 388–406.

[49] Z. Yang, K. Hu, X. Meng, Q. Tao, J. Dong, B. Liu, Q. Lu, H. Zhang, B. Sundqvist, P. Zhu, Tuning the band gap and the nitrogen content in carbon nitride materials by high temperature treatment at high pressure, Carbon 130 (2018) 170–177.

[50] E.H. Rhoderick, R.H. Williams, Metal-semiconductor Contacts, Clarendon Press, 1988.

[51] Q. Gu, Q. Jia, J. Long, Z. Gao, Heterogeneous photocatalyzed C-C cross-coupling reactions under visible-light and near-infrared light irradiation, ChemCatChem 11 (2019) 669–683.

[52] A.L. Linsebigler, G. Lu, J.T. Yates Jr, Photocatalysis on TiO_2 surfaces: principles, mechanisms, and selected results, Chem. Rev. 95 (1995) 735–758.

[53] F. Wang, C. Li, H. Chen, R. Jiang, L.-D. Sun, Q. Li, J. Wang, J.C. Yu, C.-H. Yan, Plasmonic harvesting of light energy for Suzuki coupling reactions, J. Am. Chem. Soc. 135 (2013) 5588–5601.

[54] L. Kurti, B. Czakó, Strategic Applications of Named Reactions in Organic Synthesis, Elsevier, 2005.